Progesterone and HMOX-1 promote fetal growth by CD8+ T cell modulation

María Emilia Solano,[1] Mirka Katharina Kowal,[1] Greta Eugenia O'Rourke,[1] Andrea Kristina Horst,[2] Kathrin Modest,[1] Torsten Plösch,[3] Roja Barikbin,[2] Chressen Catharina Remus,[4] Robert G. Berger,[5] Caitlin Jago,[1] Hoang Ho,[6] Gabriele Sass,[2] Victoria J. Parker,[7] John P. Lydon,[8] Francesco J. DeMayo,[8] Kurt Hecher,[1] Khalil Karimi,[2] and Petra Clara Arck[1]

[1]Department of Obstetrics and Fetal Medicine, Laboratory for Experimental Feto-Maternal Medicine, and [2]Institute of Experimental Immunology and Hepatology, University Medical Center Hamburg-Eppendorf, Hamburg, Germany. [3]Department of Obstetrics and Gynaecology, University Medical Center Groningen, University of Groningen, Groningen, Netherlands. [4]Department of Diagnostic and Interventional Radiology, University Medical Center Hamburg-Eppendorf, Hamburg, Germany. [5]Intrinsik Health Sciences Inc., Mississauga, Ontario, Canada. [6]McMaster University, Hamilton, Ontario, Canada. [7]Centre for Integrative Physiology, University of Edinburgh, Edinburgh, United Kingdom. [8]Baylor College of Medicine, Houston, Texas, USA.

Intrauterine growth restriction (IUGR) affects up to 10% of pregnancies in Western societies. IUGR is a strong predictor of reduced short-term neonatal survival and impairs long-term health in children. Placental insufficiency is often associated with IUGR; however, the molecular mechanisms involved in the pathogenesis of placental insufficiency and IUGR are largely unknown. Here, we developed a mouse model of fetal-growth restriction and placental insufficiency that is induced by a midgestational stress challenge. Compared with control animals, pregnant dams subjected to gestational stress exhibited reduced progesterone levels and placental heme oxygenase 1 (*Hmox1*) expression and increased methylation at distinct regions of the placental *Hmox1* promoter. These stress-triggered changes were accompanied by an altered CD8+ T cell response, as evidenced by a reduction of tolerogenic CD8+CD122+ T cells and an increase of cytotoxic CD8+ T cells. Using progesterone receptor– or *Hmox1*-deficient mice, we identified progesterone as an upstream modulator of placental *Hmox1* expression. Supplementation of progesterone or depletion of CD8+ T cells revealed that progesterone suppresses CD8+ T cell cytotoxicity, whereas the generation of CD8+CD122+ T cells is supported by *Hmox1* and ameliorates fetal-growth restriction in *Hmox1* deficiency. These observations in mice could promote the identification of pregnancies at risk for IUGR and the generation of clinical interventional strategies.

Introduction

Intrauterine growth restriction (IUGR) in humans is associated with poor fetal growth and impaired fetal development. In Western societies, the incidence of IUGR varies to between 3% and 10% of the total population, with an unprecedented increase observed over the last decades (1–4). IUGR not only strongly predicts reduced short-term neonatal survival (5), but is also associated with adverse long-term health outcomes, including increased risk for cardiovascular disease and chronic immune disease (6–8). Maternal factors known to influence fetal development, including age, weight, race, socioeconomic status, nutrition, or smoking, have also been associated with IUGR (3, 9–10). Moreover, high maternal stress perception is increasingly recognized as enhancing the risk for IUGR (11–16). Placental insufficiency is a known contributor to IUGR (17, 18). To date, however, molecular mechanisms leading to IUGR and placental insufficiency are still largely unknown.

Fine-tuned maternal endocrine and immune adaptations interact during pregnancy to create a tolerogenic intrauterine environment that promotes placental development and fetal growth in eutherian mammals (18–21). The placenta mediates the interactions between mother and fetus by providing the fetus with nutrients and oxygen and allowing waste exchange between the fetal and maternal systems (19, 22). This is largely possible through the formation of a complex placental vascular net that closely approximates maternal blood sinuses and fetal capillaries (19, 22). Furthermore, in the mouse placenta, trophoblast cells, such as the parietal giant cells (pGCs), produce a number of paracrine and endocrine hormones, which can stimulate ovarian progesterone production (19, 20).

Progesterone (the progestation hormone) is pivotal for pregnancy success. When pregnancy commences, progesterone stimulates decidualization of endometrial stromal cells and maternal immune adaptation to pregnancy; it subsequently sustains uterine quiescence throughout pregnancy (23–25). There is a significant rise of progesterone during pregnancy, and even subtle deficits can affect the course of pregnancy by increasing the risk of miscarriage (26) or reduced birth weight (27, 28).

In addition to progesterone, emerging evidence suggests that heme oxygenase 1 (HMOX-1), an enzyme that catalyzes the degradation of heme into carbon monoxide, biliverdin, and iron, is also a critical mediator of pregnancy maintenance and placental function (29–32). HMOX-1 is expressed in most tissues, including the placenta in mice and humans (29, 31), and acts as a critical factor for promoting vasculature formation and immune homeo-

Authorship note: Mirka Katharina Kowal and Greta Eugenia O'Rourke contributed equally to this work.
Conflict of interest: The authors have declared that no conflict of interest exists.
Submitted: November 18, 2014; **Accepted:** January 29, 2015.
Reference information: *J Clin Invest*. 2015;125(4):1726–1738. doi:10.1172/JCI68140.

stasis by inhibiting overshooting reactions in a number of tissues in the body (31–33). Both progesterone and HMOX-1 can suppress $CD4^+$ effector T cell responses and induce the generation of $CD4^+$ Tregs (34–37), which also promote maternal immune tolerance to the fetus (38, 39). Maternal $CD8^+$ T cell responses can also affect placental function (40–42). Recent studies in mouse models have indicated that the presence of the naturally occurring $CD8^+$ T cell subset $CD8^+CD122^+$ T cells is capable of suppressing inflammation in autoimmunity, transplantation, and other inflammatory conditions (43–45). However, to date, the mediators involved in the generation of $CD8^+CD122^+$ T cells and their functional role in pregnancy maintenance remain unknown.

The aim of the present study was to develop a mouse model in order to advance our understanding of the underlying molecular mechanisms of fetal-growth restriction. It was our goal to identify an interaction and functional hierarchy between the 2 promoters of pregnancy maintenance, maternal progesterone and placental HMOX-1, as well as their effect on the $CD8^+$ T cell response in the context of fetal growth.

Results

Fetal-growth restriction and features of placental insufficiency are caused by midgestational stress challenge in mice. Maternal stress is known to impair fetal development (13–16). Early during gestation, exposing mouse dams to a sound stress challenge is associated with an increase in the fetal loss rate (25, 46). To develop a mouse model of fetal-growth restriction and placental insufficiency, we exposed pregnant dams to sound stress at midgestation (gestation day [gd12.5]), when placentation is largely completed. We rechallenged the dams with sound stress on gd14.5. Using this intervention, we observed a significant delay in fetal development according to the Theiler stage (TS) criteria measurements on gd16.5 (Figure 1, A–C). Average fetal weight was also significantly decreased in stress-challenged fetuses compared with nonstressed controls (Figure 1D). The midgestational stress challenge did not affect litter size, fetal loss, or gestational length (Figure 1E and Supplemental Figure 1, A and B; supplemental material available online with this article; doi:10.1172/JCI68140DS1). Following parturition, a significant decrease in neonatal weight was also observed on postnatal day 2 (Figure 1F).

Initially a significant decrease in placental weight was observed in stress-challenged litters on gd14.5; however, on gd16.5, placental weights returned to values similar to those seen in control mice (Supplemental Figure 1C). The surfaces of 2 placental functional areas, the labyrinth and junctional zone, were evaluated histomorphologically in order to calculate the labyrinth/junctional zone (L/Jz) ratio. The L/Jz ratio has been used as a marker for placental function (47). We observed significant changes of the L/Jz ratio on gd13.5 and gd14.5, indicative of a relative labyrinth reduction in response to stress challenge. Commencing on gd15.5, the L/Jz ratio was then inverted due to a relative increase of the labyrinth (Figure 1, G and I). These histomorphological findings were confirmed by MRI of the placentas taken on gd16.5 (Supplemental Figure 1, D and E, and Supplemental Methods). Since the labyrinth comprises a complex vascular network promoting nutrient and oxygen transfer to the fetus (19, 22), we evaluated fetal vessel density, identified by the presence of $CD34^+$ vessels, in the placental labyrinth. We focused on distal areas of the labyrinth, where blood perfusion is less affected by the high blood flow along the central arterial placental canal or the chorionic plate vessels, as identified by MRI (Supplemental Figure 1E). Labyrinth vessel density increased during the progression of pregnancy in control animals, showing a substantial increase from gd15.5 to gd16.5. On gd14.5, a decrease in vessel density was present in stress-challenged animals; this was reversed on gd16.5 (Figure 1, H and I).

Additional characterization of the placenta (Supplemental Methods) revealed that the frequency of lymphatic vascular endothelial hyaluronan receptor-1^+ ($LYVE\text{-}1^+$) vessels within the vascular net of the labyrinth was significantly reduced in response to stress challenge, commencing on gd15.5 (Supplemental Figure 1, F and G). Furthermore, placental expression of carcinoembryonic antigen-related cell adhesion molecule-1 (CEACAM-1), a marker facilitating the identification of glycogen trophoblast cells, was decreased in response to stress (Supplemental Figure 1, H and I). No differences in the frequency of pGC in placental tissue were observed between control and stress-challenged groups (Supplemental Figure 1, H and J).

Collectively, these data indicate that the prenatal stress challenge at midgestation in mice resulted in fetal-growth restrictions that were associated with markers of placental insufficiency, including reduced vascularization, similar to the clinical signs of IUGR in humans.

Progesterone and placental Hmox1 expression are reduced and $CD8^+$ T cell response is altered in fetal-growth restriction. We observed a significant decrease in serum progesterone levels in stress-challenged dams (Figure 2A). Further evidence of stress-related decreases in progesterone levels was provided through kinetic studies using urine samples (Supplemental Figure 2A and Supplemental Methods). Reduced placental expression of proliferin and placental lactogen II (*Prl3b1*) suggested reduced placental endocrine activity (20) in response to stress (Supplemental Figure 2, B–D, and Supplemental Methods). An increase in pGC death accounting for these alterations was excluded, as apoptotic pGCs did not differ between groups (Supplemental Figure 2, E and F). We also observed a significant decrease in ovarian expression of 3β-hydroxysteroid dehydrogenase (*Hsd3b1*), which converts pregnenolone to progesterone, and a reduction of the ovarian steroidogenic acute regulatory protein (*Star*), which transports cholesterol from the outer to the inner mitochondrial membrane (Supplemental Figure 2, G and H). These findings suggest that progesterone synthesis was impaired in ovaries of stress-challenged mice. As ovarian expression of 20αHSD (*Akr1c18*) was very low and there were no significant differences between control and stressed animals at midgestation (data not shown), the observed decrease in progesterone levels was not due to changes in progesterone metabolism rates.

A direct link between progesterone availability and fetal growth was confirmed through experiments with progesterone receptor transgenic (*Pgr*) mice. Upon mating of $Pgr^{+/-}$ females to $Pgr^{+/-}$ males, which results in implantations of $Pgr^{+/+}$, $Pgr^{+/-}$, and $Pgr^{-/-}$ genotypes following Mendelian distribution (Supplemental Figure 2I), there was a significant reduction of fetal weight in implantations with the $Pgr^{-/-}$ genotype compared with $Pgr^{+/+}$ fetuses in the same litter (Figure 2B). Further, these changes in fetal weight were accompanied by reduced placental L/Jz ratios due to a decrease in labyrinth size (Figure 2C).

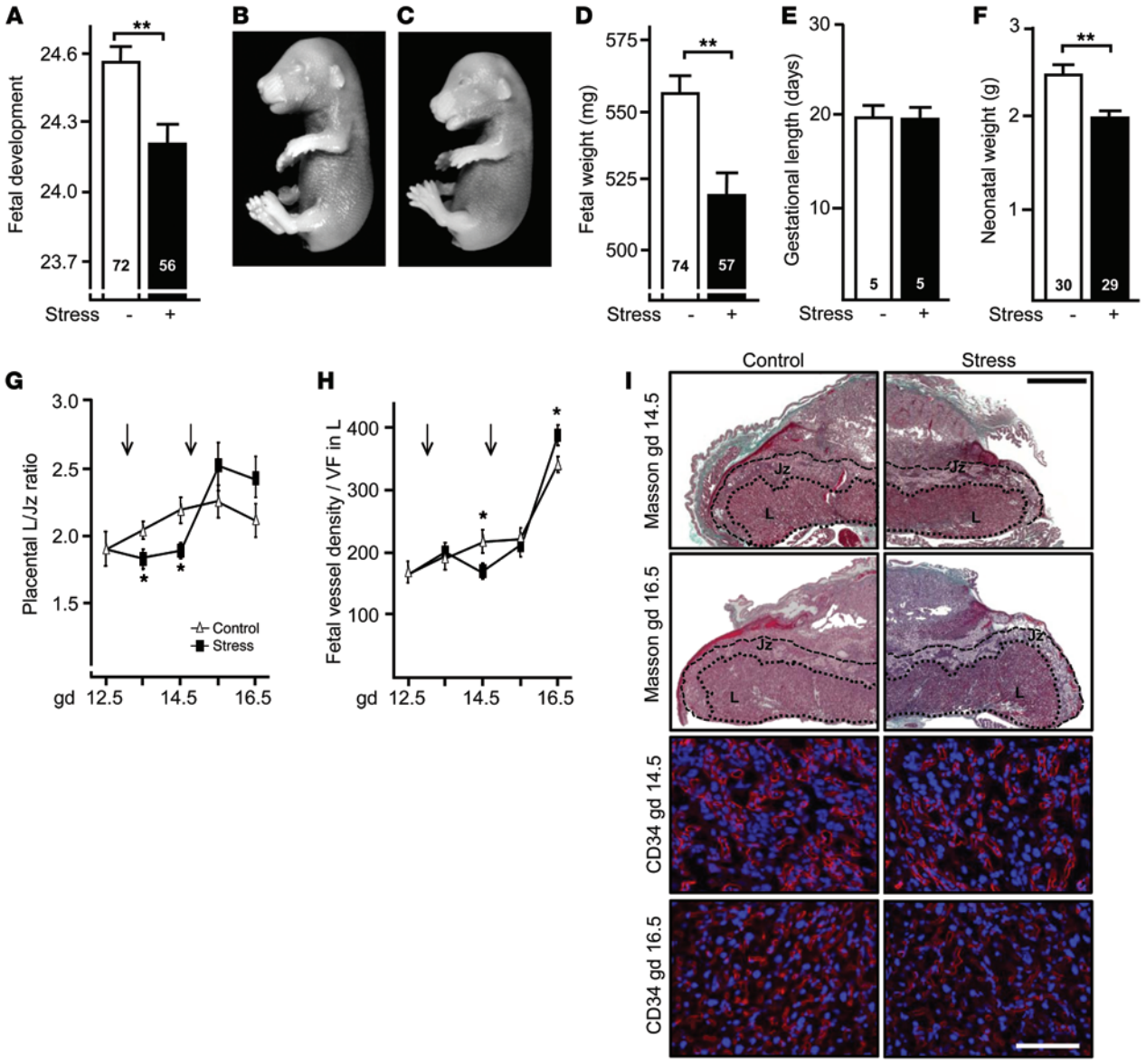

Figure 1. Prenatal stress results in fetal-growth restriction and placental insufficiency. (**A**) Fetal development was scored on gd16.5 according to TS criteria. (**B**) Representative photograph of a TS 25 fetus on gd16.5 depicting parallel fingers and toes, fused eyelids, and thickened skin that forms wrinkles. (**C**) Photograph of a prenatally stress-challenged gd16.5 fetus in TS 24, exhibiting divergent toes and fingers, open eyelids, and thin skin without wrinkles. (**D**) Fetal weight on gd16.5, (**E**) gestational length, and (**F**) postnatal day 2 weight from control and prenatally stress-challenged litters. (**G**) L/Jz ratio, obtained upon histomorphometric analyses of Masson-stained placental tissue sections harvested on gd12.5 to gd16.5. (**H**) Fetal vessel density in the placental labyrinth, calculated as $CD34^+$ vessel number per visual field (VF). Arrows indicate the beginning of the 24-hour exposure to sound stress. (**I**) Representative photomicrographs depict midsagittal sections of gd14.5 and gd16.5 placental tissue. Top panels: Masson staining allows differentiating the labyrinth and junctional zone. Bottom panels: $CD34^+$ (red) fetal vessels in the placental labyrinth labeled by immunofluorescence; cell nuclei were counterstained with DAPI (blue). Scale bars: 1 mm (top panels); 0.1 mm (lower panels). The *n* used in each group and experiment is depicted inside the bars (**A** and **D**–**F**). For parts **G** and **H**, a minimum of 8 placentas per group and gd were quantified to identify differences between groups. (**A** and **D**–**H**) Data represent the mean ± SEM. $^*P \leq 0.05$; $^{**}P \leq 0.001$; Mann-Whitney *U* test (**D**–**H**) and χ^2 test (**A**) were used to calculate the statistical differences between groups (**A**: χ^2 (2,*N* = 128) = 9.357).

Stress-challenged females also showed a significant decrease in placental *Hmox1* mRNA expression (Figure 2D). HMOX-1 is also expressed on protein levels in the placental labyrinth, pGC, placenta-infiltrating leukocytes, and in decidua and myometrium (Figure 2E and Supplemental Figure 3, A and B). DNA methylation in a CpG island around the transcription start site of the *Hmox1* gene was analyzed using pyrosequencing, as altered methylation could account for the downregulation of placental *Hmox1* expression. Overall, regardless of stress exposure, we observed low levels of CpG methylation of the *Hmox1* promoter region in the placenta. However, the methylation in 2 CpG positions was significantly increased in the placentas of prenatally stressed females (Figure 2F). Interestingly, the first of these CpG positions (–109) is adjacent to the binding site for the transcription factor specificity protein-1 (SP-1) (Supplemental Table 4).

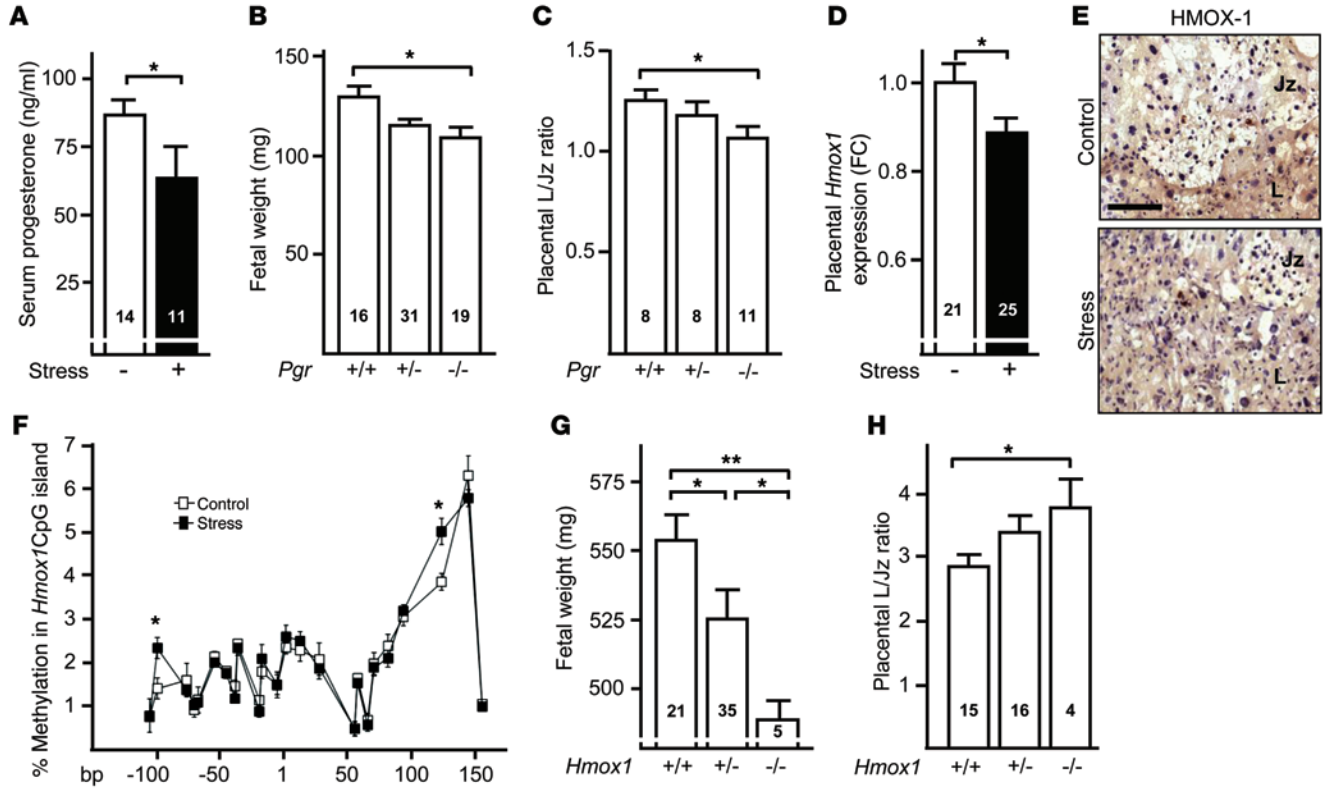

Figure 2. Progesterone levels and placental *Hmox1* expression are reduced in fetal-growth restriction. (**A**) Levels of serum progesterone in control and stress-challenged dams on gd16.5, as analyzed by RIA. (**B**) Fetal weight and (**C**) placental L/Jz ratio in gd13.5 placentas resulting from $Pgr^{+/-}$ × $Pgr^{+/-}$ mating combinations. The fetal/placental *Pgr* genotypes are provided under the respective bars. (**D**) Fold change (FC) in *Hmox1* mRNA expression quantified by RT-PCR in placental samples from control and stress-challenged pregnancies on gd16.5. (**E**) Photomicrographs showing detail of the labyrinth and junctional zone areas of representative placental tissue sections upon immunohistochemical detection of HMOX-1 (appears brown). Tissue was counterstained with hematoxylin. Scale bar: 0.1 mm. (**F**) Pyrosequencing methylation analysis of a CpG island in the *Hmox1* promoter region in placenta samples from control and stress-challenged dams on gd16.5 ($n \geq 7$). The CpG island locates 110-bp upstream and 172-bp downstream from the transcriptional start site, which is denoted as 1. (**G**) Fetal weight in offspring arising from $Hmox1^{+/-}$ × $Hmox1^{+/-}$ mating combinations. The fetal/placental *Hmox1* genotypes are provided under the respective bars. (**H**) L/Jz ratio obtained from analyses of Masson-stained placental tissue sections taken on gd16.5 from $Hmox1^{+/-}$ × $Hmox1^{+/-}$ mating combinations. The *n* used in each group and experiment is depicted inside the bars (**A**–**D** and **G**–**H**). Data are presented as mean ± SEM per respective group. $^{*}P \leq 0.05$; $^{**}P \leq 0.01$. Analyses were performed using Mann-Whitney *U* test (**A**, **D**, and **F**) and the Kruskal-Wallis test (**B**, **C**, **G**, and **H**).

We then sought to confirm the link between reduced placental *Hmox1* expression and fetal weight by mating $Hmox1^{+/-}$ females with $Hmox1^{+/-}$ males. This mating combination resulted in fetuses with $Hmox1^{+/+}$, $Hmox1^{+/-}$, and $Hmox1^{-/-}$ genotypes. The Mendelian distribution — as expected from published evidence (31) — is disrupted in this mating combination, as shown through the reduced frequency of implantation sites of the $Hmox1^{-/-}$ genotype (13% instead of an expected 25%). Reduced levels or a complete absence of *Hmox1* expression in $Hmox1^{+/-}$ and $Hmox1^{-/-}$ placentas, respectively, was associated with a significant reduction in fetal weight (Figure 2G). $Hmox1^{-/-}$ implantation sites also had increased placental L/Jz ratios when compared with $Hmox1^{+/+}$ (Figure 2H). However, similar to the effect of stress on the labyrinth in WT mice, the labyrinth area was also reduced in $Hmox1^{-/-}$ mice. Therefore, the unexpected increase of the L/Jz ratio in $Hmox1^{-/-}$ placentas was due to a disproportionate decrease of the junctional zone.

Based on the well-known functions of progesterone and HMOX-1 in modulating immune responses in conjunction with the observed responses to a stress challenge reported here, we assessed the effect of stress challenge on distinct immune cell subsets in uterus-draining lymph nodes. No changes in the proportion of $CD4^+$ T cells and $CD4^+$ Tregs were found (Figure 3, A and B), but there was an overall increase in $CD8^+$ T cell frequencies in response to the stress challenge (Figure 3C). This $CD8^+$ T cell increase was associated with a decrease in the $CD8^+CD122^+$ T cell subset (Figure 3, D and E) and a skew toward cytotoxic, $CD107\alpha^+IFN\text{-}\gamma^+CD8^+$ T cells in response to the stress challenge (Figure 3, F and G). Moreover, we observed an increase in dendritic cells ($CD11c^+CD11b^{neg}$) and $DX5^+$ NK cells in animals exposed to the stress challenge (Figure 3, H and I), albeit at very low frequencies compared with T cells.

Progesterone is an upstream modulator of placental Hmox1 expression. As shown in Figure 2, we observed impaired fetal growth and signs of placental insufficiency in pregnancies with low levels of progesterone and reduced placental expression of *Hmox1* in dams exposed to a stress challenge. These findings were strengthened by our observations of fetal-growth restriction in *Pgr* and *Hmox1* mutant mice. Therefore, we aimed to test for an interaction and determine the functional hierarchy between these 2 markers. We first assessed placental *Hmox1* in $Pgr^{+/-}$ females mated to $Pgr^{+/-}$

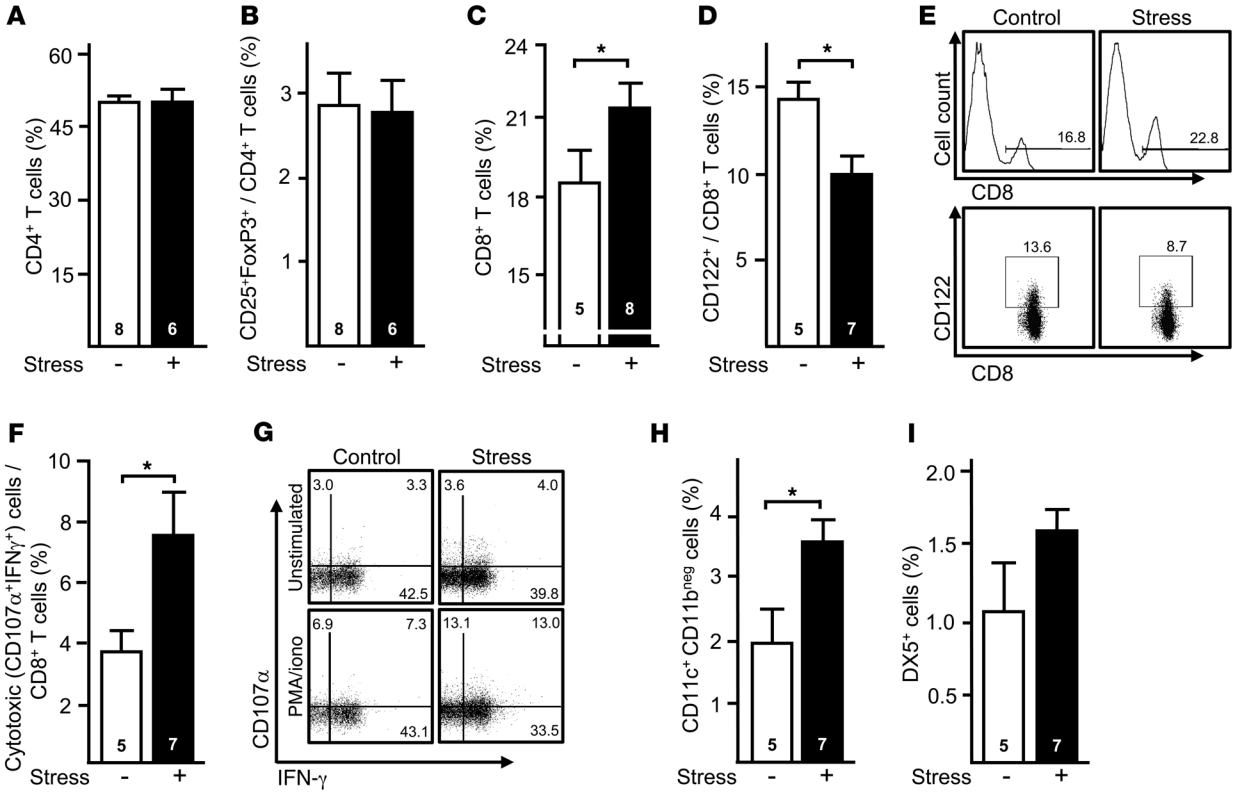

Figure 3. Effect of prenatal stress challenge on maternal immune cells. Flow-cytometric analysis of (**A**) CD4$^+$ T cells or (**B**) CD25$^+$FoxP3$^+$CD4$^+$ Tregs in uterus-draining lymph nodes harvested from gd16.5 control and stress-challenged BALB/c dams. Frequency of CD8$^+$ T cells (**C**) and of CD8$^+$CD122$^+$ T cells (**D**) in lymph nodes from control and stress-challenged dams. (**E**) In the top panels, the histograms depict the gating strategy used to determine the CD8$^+$ T cell population, whereas the lower panels show the CD122$^+$ cell subset within the CD8$^+$ T cells. (**F**) CD8$^+$ T cell cytotoxicity, as indicated by CD107α (which mirrors the degranulation of lytic granules) and intracellular levels of IFN-γ. Cytotoxicity was calculated as the difference (Δ) in the positivity for CD107α and IFN-γ between PMA/ionomycin-stimulated and unstimulated CD8$^+$ T cells evaluated by flow cytometry. (**G**) Representative dot plots for CD107α and IFN-γ in unstimulated and PMA/ionomycin-stimulated CD8$^+$ T cells harvested from uterine lymph nodes of control and stress-challenged dams on gd16.5. CD11c$^+$CD11b^{neg} dendritic cells (**H**) and DX5$^+$ NK cells (**I**) were found in low frequencies in the uterus-draining lymph nodes. Cell frequencies in **A**, **C**, **H**, and **I** are provided as percentages of cells in the leukocyte gate, whereas in **B** and **D**, they are provided as percentages of CD4$^+$ T and CD8$^+$ T cells, respectively. The *n* used in each group and experiment is depicted inside the bars (**A**–**D**, **F**, **H**, and **I**). Bars represent mean ± SEM. $^*P \leq 0.05$, analyzed by Mann-Whitney *U* test.

males and observed a significant reduction in *Hmox1* expression in *Pgr*$^{-/-}$ placentas compared with *Pgr*$^{+/+}$ placentas (Figure 4A). Further, when stress-challenged dams were administered supplemental progesterone, an upregulation of placental *Hmox1* expression, along with an improvement in fetal weight and development, was observed. The placental L/Jz ratio was restored, and the stress-induced skew toward CD8$^+$ T cell cytotoxicity was not seen in stress-challenged dams following the administration of progesterone (Figure 4B). Surprisingly, supplemental progesterone had no impact on the proportion of CD8$^+$CD122$^+$ T cells detected. These findings strongly support an upstream function of progesterone in regulating placental *Hmox1* expression and dampening CD8$^+$ T cell cytotoxicity, while CD8$^+$CD122$^+$ T cells were refractory to the direct effect of progesterone. It does not appear that *Hmox1* modulates progesterone levels during murine gestation, as levels of progesterone were similar in WT mice and *Hmox1*$^{+/-}$ pregnant females (Figure 4C).

Generation of CD8$^+$CD122$^+$ T cells is supported by HMOX-1 and compensates for Hmox1 deficiency–related fetal-growth restriction. Given that we observed a decrease of CD8$^+$CD122$^+$ T cells in response to stress, which administration of supplemental progesterone failed to restore, we aimed to identify pathways promoting the generation of CD8$^+$CD122$^+$ T cells. A reduction in the proportion of CD8$^+$CD122$^+$ T cells in uterus-draining lymph nodes of *Pgr*$^{+/-}$ mice on gd13.5 was observed when compared with WT mice (Figure 5A). Similarly, the proportion of CD8$^+$CD122$^+$ T cells was significantly lower in uterus-draining lymph nodes of *Hmox1*$^{+/-}$ mice compared with WT mice (Figure 5B). Since progesterone levels were similar in *Hmox1*$^{+/-}$ and *Hmox1*$^{+/+}$ mice, these observations suggest that *Hmox1*, while sustained by progesterone, promotes the generation of CD8$^+$CD122$^+$ T cells. To strengthen this, we tested the effect of experimental HMOX-1 upregulation by cobalt protoporphyrin (CoPP) administration (48). Here, we focused on nonpregnant mice, since the options to use CoPP during pregnancy are very limited, due to its severe endocrine side effects (49, 50) and possible teratogenicity. Indeed, CoPP injection resulted in a significant increase of CD8$^+$CD122$^+$ T cells in uterus-draining lymph nodes (Figure 5C), confirming the notion that *Hmox1* promotes the generation of CD8$^+$CD122$^+$ T cells.

We then assessed the functional role of CD8$^+$CD122$^+$ T cells in fetal growth and placental function by transferring CD8$^+$CD122$^+$

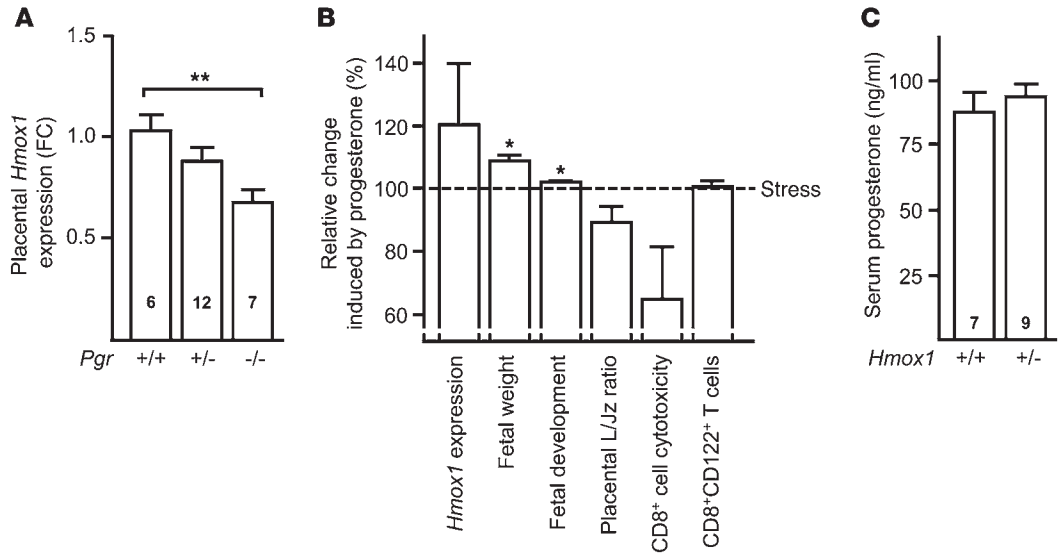

Figure 4. Progesterone is an upstream modulator of placental *Hmox1* expression. (**A**) RT-PCR quantification in $Pgr^{+/+}$, $Pgr^{+/-}$, and $Pgr^{-/-}$ placentas resulting from $Pgr^{+/-}$ matings revealed a significantly reduced *Hmox1* expression in $Pgr^{-/-}$ implantations, compared with $Pgr^{+/+}$ implantations. (**B**) Effect of progesterone supplementation on gd11.5, gd13.5, and gd15.5 in stressed mice on placental and fetal parameters, compared with stressed mice without progesterone supplementation. From left to right: placental *Hmox1* expression assessed by RT-PCR (n = 8 in progesterone supplementation plus stress/n = 9 in stress only), fetal weight and TS development (n = 60/n = 56), placental L/Jz ratio assessed by histomorphology (n = 12/n = 14), $CD8^+$ T cell cytotoxicity (n = 5/n = 7), and $CD8^+CD122^+$ T cell frequencies (n = 5/n = 7) analyzed by flow cytometry. Results are provided as relative change induced by progesterone supplementation over stress. Data were calculated by normalizing the values obtained for each variable upon progesterone supplementation to the respective value in stress-challenged nonprogesterone supplemented dams. (**C**) Levels of serum progesterone on gd16.5 in $Hmox1^{+/+}$ and $Hmox1^{+/-}$ BALB/c dams. (**A** and **B**) Fold change over control expression was calculated using *Hprt* as housekeeping gene and the ΔΔCt method. The n used in each group and experiment is depicted inside the bars (**A** and **C**). Bars represent mean ± SEM. $^*P \le 0.05$; $^{**}P \le 0.01$, analyzed by Mann-Whitney U test.

T cells into $Hmox1^{+/-}$-mated $Hmox1^{+/-}$ females. Upon $CD8^+CD122^+$ T cell transfer, a significant improvement in fetal weight could be observed in fetuses of $Hmox1^{-/-}$ genotypes compared with $Hmox1^{-/-}$ fetuses receiving sham treatment (Figure 5D). This $CD8^+CD122^+$ T cell adoptive transfer–induced improvement of fetal weight was accompanied by an increased placental and labyrinth area and a profound increase of the junctional zone (data not shown). This resulted in a decreased L/Jz ratio (Figure 5E). Strikingly, upon transfer of $CD8^+CD122^+$ T cells, the $Hmox1^{-/-}$ placentas showed a significant increase in vascularization (Figure 5, F and G). This important role of $CD8^+$ T cells in ensuring fetal growth was further supported by a significant reduction in fetal weight and development and placental L/Jz ratio upon $CD8^+$ T cell depletion, which abrogated the improved fetal weight induced by supplemental progesterone (Figure 5, H–J).

Discussion

Here, we introduce a mouse model of fetal-growth restriction triggered by stress challenge during midgestation. The fetal-growth restriction was accompanied by signs of placental insufficiency, similar to IUGR in humans. In this mouse model, progesterone and placental *Hmox1* expression were reduced, and methylation of the *Hmox1* promoter was altered. Using this stress model along with *Pgr* and *Hmox1* transgenic mice, we were able to provide evidence that progesterone upregulates placental *Hmox1* expression. Moreover, we identified a dichotomous $CD8^+$ T cell response in stress-challenged dams, as shown by an increase in the proportion of cytotoxic $CD8^+$ T cells along with reduced frequencies of $CD8^+$ T cells coexpressing CD122. We provide evidence that the generation of $CD8^+CD122^+$ T cells is promoted by *Hmox1* and that adoptive transfer of $CD8^+CD122^+$ T cells ameliorated fetal growth and placental vascularization in $Hmox1^{-/-}$ implantations. The conceptual scenario arising from these findings is depicted in Figure 5K.

Placental insufficiency and fetal growth restriction have previously been observed in a number of mouse models. However, these models were largely restricted to the use of genetically engineered mice lacking particular genes, such as endothelial nitric oxide synthase (51, 52) and *Hmox1* (31). Compared with these, the model for fetal-growth restriction upon stress challenge used here is of greater clinical relevance, given that the causative mechanisms were mounted endogenously.

One key mechanism leading to fetal-growth restriction that we observed involved changes in progesterone levels. Decreased levels of progesterone were observed in response to the stress challenge, a response that appears to be highly conserved across species (26, 46, 53) despite species-specific differences in progesterone production. Low placenta-dependent stimulation with *Prl3b1* and low ovarian expression of the progesterone-synthesizing enzymes *Star* and *Hsd3b1* indicate that the stress-induced decrease of progesterone results from a reduction of progesterone synthesis rather than altered rates of progesterone metabolism via 20αHSD (*Akr1c18*). However, the ovarian expression of 20αHSD we observed was very low in all groups and may have limited the detection of any potential differences among groups. Moreover, inflammatory markers acting directly at the corpus luteum have been linked to an inhibition of progesterone secre-

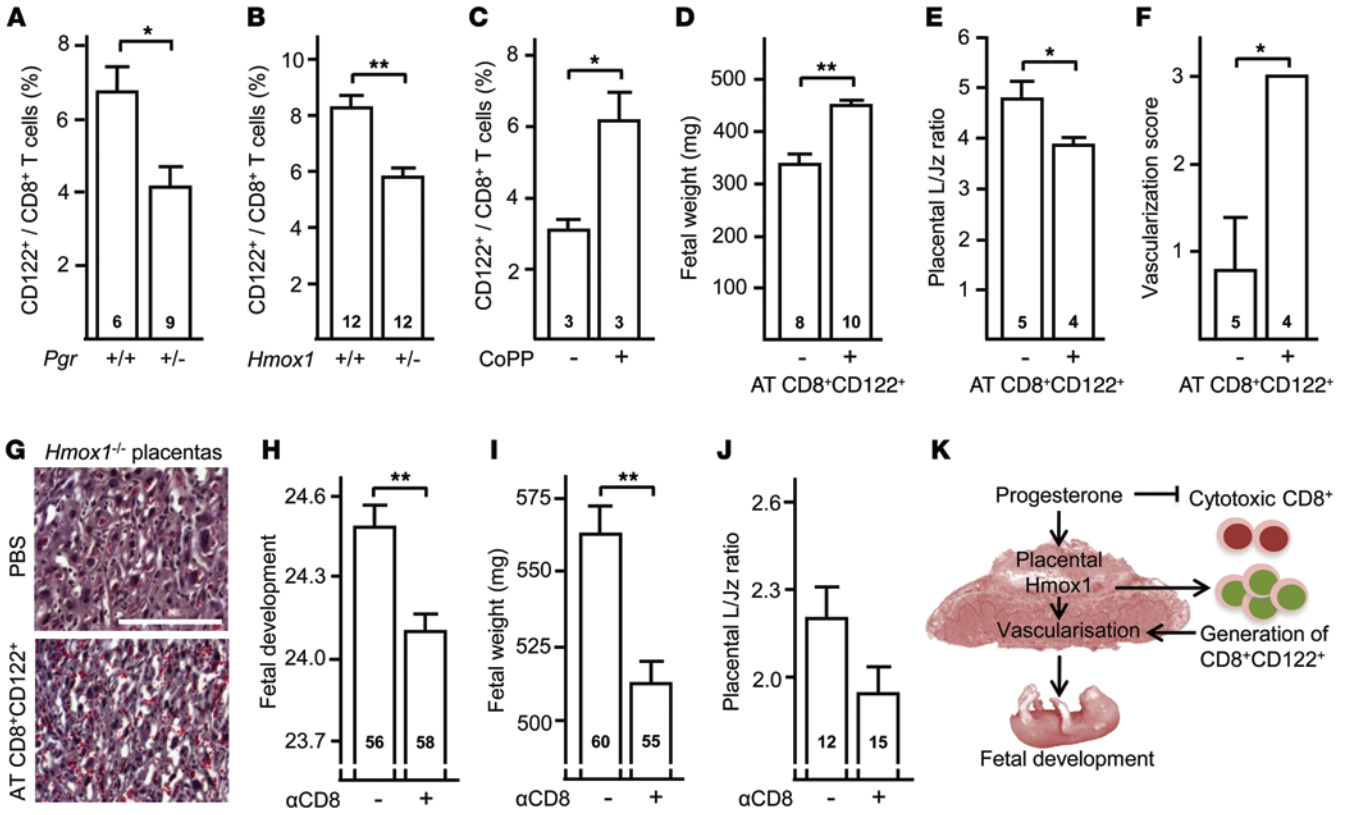

Figure 5. Generation of CD8⁺CD122⁺ T cells is supported by HMOX-1 and contributes to compensation for fetal-growth restriction. Flow-cytometric quantification of CD8⁺CD122⁺ T cells in uterus-draining lymph nodes from *Pgr*$^{+/-}$ mice on gd13.5 (**A**) and *Hmox1*$^{+/-}$ mice on gd16.5 (**B**), compared with their respective WT control on the same gd. (**C**) CD122⁺CD8⁺ T cell frequencies in uterus-draining lymph nodes from control and CoPP-treated nonpregnant female BALB/c mice. Effect of the adoptive transfer (AT) of 0.3 × 10^6 CD8⁺CD122⁺ T cells in *Hmox1*$^{-/-}$ implantations resulting from *Hmox1*$^{+/-}$ matings (**D**–**G**). On gd16.5, fetal weight (**D**) and placental L/Jz ratio (**E**) were calculated. (**F**) Placental labyrinth was also scored for the progress of vascularization (0, low; 3, high). (**G**) Representative example of a placental labyrinth scoring 0 from a PBS-injected female and of a placental labyrinth scoring 3 from a CD8⁺CD122⁺ T cell–transferred female. Scale bar: 0.1 mm. The effect of antibody-induced (αCD8: anti–Lyt 2) CD8⁺ cell depletion in stress-challenged progesterone-supplemented dams was evaluated on gd16.5 (**G**–**I**). Here, fetal development according to TS criteria (**H**), fetal weight (**I**), and placental L/Jz ratio (**J**) were calculated. (**K**) Hypothetical scenario depicting the interaction among progesterone, HMOX-1, and CD8⁺ T cells in promoting fetal development. Pointed arrows depict activation/promotion, and blunted arrows depict suppression. (**E** and **J**) Placental L/Jz ratio was calculated by quantifying the individual areas in Masson-stained placental tissue sections. The *n* used in each group and experiment is depicted inside the bars (**A**–**F** and **H**–**J**). Bars represent the mean ± SEM. **P* ≤ 0.05; ***P* ≤ 0.001, analyzed by Mann-Whitney *U* test.

tion (54, 55), since the inflammatory stimulus can induce apoptosis in luteal cells and endothelial cells in the corpus luteum. Moreover, macrophages have recently been identified as critically supporting the vascular network required for corpus luteum integrity and production of progesterone during early pregnancy in mice (56). Since we observed an increased inflammatory response upon stress challenge in the present study, disruption of the corpus luteum integrity directly by these inflammatory markers or due to an altered phenotype of macrophages may account for the decreased progesterone production.

In human pregnancy, the ovaries initially produce progesterone until a shift from luteal to placental progesterone production occurs around gestation week 6. The placenta is subsequently the main source of progesterone until term. Insights into how stress challenges affect the production of progesterone or its sites of production are still unknown, as progesterone levels are not routinely assessed in human pregnancies.

We provide evidence that the degree of placental *Hmox1* expression is dependent on the availability of progesterone. Indeed, our experiments in *Pgr* transgenic mice show that placental *Hmox1* expression was reduced if progesterone was unavailable due to the reduction or complete absence of the progesterone receptor. Therefore, the low levels of placental *Hmox1* expression following the stress challenge, along with placental insufficiency and fetal-growth restriction, may result from low levels of progesterone.

We also reported an epigenetic modulation of the placental *Hmox1* promoter that was associated with an increase in methylation in response to stress challenge. Increased methylation levels could account for the decreased placental expression of *Hmox1* (57) in response to stress. However, this observation does not yet explain how progesterone can modulate *Hmox1* expression. To identify potential pathways, we searched for possible progesterone receptor–binding sites within the promoter region of *Hmox1* and showed that the region does not include the known progesterone response element (PRE) or the estrogen and glucocorticoid response elements (58–61). This does not exclude the possibility of such response elements within the promoter region of *Hmox1*, as our search was restricted to the sequences identified to date.

Furthermore, among the transcription factors that control *Hmox1* promoter, SP-1 can interact with the progesterone receptor in several tissues (62). Of note, one of the differentially methylated CpG positions seen in response to stress challenge is adjacent to the binding site for the SP-1. Hence, additional work is needed to determine whether SP-1 and the progesterone receptor interact in the placenta and whether this potential interaction is affected by the altered methylation of the *Hmox1* promoter.

Functionally, placental HMOX-1 promotes placental vascularization of the labyrinth (63), as shown by decreased microvasculature vessel volumes in the labyrinth region of *Hmox1*$^{+/-}$ placentas compared with placentas from WT mice. This altered vascularization in *Hmox1*$^{+/-}$ placentas is linked to a decrease of proangiogenic factors in the placenta (63). These observations are in line with our findings in stressed mice, in which reduced placental *Hmox1* expression was associated with a substantially altered placental vascularization.

In human pregnancies, HMOX-1 is expressed in the placenta and decidua (29, 64–69). Placental HMOX-1 expression has been described as being significantly higher in term human placentas (66), when levels of progesterone as well as estradiol are significantly higher than in the first trimester. This supports the notion that HMOX-1 is modulated by progesterone during human pregnancies (64–66). The functional role of placental HMOX-1 in promoting vascularization during normally progressing pregnancies, or its potential modulation in pregnancy pathologies such as IUGR, remains unclear, probably due to the use of tissue from preterm versus full-term pregnancies, low sample numbers, tissue heterogeneity, or different detection methods. However, the importance of HMOX-1 in human pregnancies may be deduced from a case report describing how a HMOX-1 deficiency (resulting from a spontaneous gene mutation in a male child) was associated with growth restriction (69). Currently, it is not an option to routinely assess placental HMOX-1 expression during human pregnancies. This limitation increases the importance of our finding that progesterone is an upstream modulator of placental *Hmox1*, as progesterone levels can be readily monitored during pregnancy as a potential proxy for placental *Hmox1* expression.

A dichotomous CD8$^+$ T cell response with decreased CD8$^+$CD122$^+$ T cell frequencies and increased frequencies of cytotoxic CD8$^+$ T cells in stress-challenged dams was also reported here. It has been proposed that progesterone, via the progesterone receptor and glucocorticoid receptor–dependent pathways (70), modulates the immune response during pregnancy, including CD4$^+$ and CD8$^+$ T cell differentiation (25, 46, 71). Interestingly, compared with WT mice, CD4$^+$ T cells from *Pgr*$^{-/-}$ mice express lower levels of TGF-β1 (35) and produce significantly more IFN-γ upon stimulation (36). This is in line with our findings about the CD8$^+$ T cell response in stress-challenged mice, where progesterone supplementation reversed CD8$^+$ T cell cytotoxicity. Together, these findings suggest that progesterone significantly dampens CD4$^+$ and CD8$^+$ T cell–mediated inflammation, potentially by opposing the proinflammatory activity of estrogen (72). Reduced levels of progesterone, as seen in response to stress challenge, may affect additional immune cell subsets or decidual markers in mice, such as in dendritic cells, NK cells, or Galectin-1, which can contribute to an impaired pregnancy outcome (25, 34).

Surprisingly, there was only a weak effect of supplemental progesterone administration on the proportion of CD8$^+$CD122$^+$ T cells. Interestingly, the proportion of CD8$^+$CD122$^+$ T cells decreased in *Pgr*$^{+/-}$ mice as well as in *Hmox1*$^{+/-}$ mice. In the latter, progesterone levels were similar to those in *Hmox1*$^{+/+}$ mice. We therefore propose that the generation of CD8$^+$CD122$^+$ T cells during pregnancy is largely triggered by HMOX-1, while progesterone strongly dampens an inflammatory CD8$^+$ T cell response during pregnancy. This notion is underscored by the absence of PRE in the CD122 promoter region. Clearly, it is difficult to tease apart the differential modulation and generation of the CD8$^+$CD122$^+$ T cell response during pregnancy, as CD8$^+$CD122$^+$ T cell frequencies remained low upon supplemental progesterone and associated placental *Hmox1* upregulation in stress-challenged dams. This observation suggests that *Hmox1*-independent mechanisms, such as direct effects on maternal thymus (73, 74), low levels of TGF-β (75), or selective glucocorticoid-induced CD8$^+$ Treg apoptosis in response to stress, could account for the impaired generation of this cell subset.

In a number of experimental models in mice, CD8$^+$CD122$^+$ T cells have been shown to be indispensable for sustaining immune homeostasis, including the induction of tolerance or suppression of autoimmunity (44, 45, 76, 77). Insights arising from *Cd122*$^{-/-}$ mouse studies support the functional role of this marker in maintaining immune homeostasis, as *Cd122*$^{-/-}$ mice spontaneously develop severe hyperimmunity (44, 45, 78, 79). Moreover, CD8$^+$CD122$^+$ Tregs can maintain homeostasis of CD8$^+$ T cells by controlling CD8$^+$ T cell activation in vivo and in vitro, mirrored by dampened IFN-γ production and suppression of CD8$^+$CD122^{lo} T cell proliferation (45, 78). In addition, CD8$^+$ T cells with regulatory functions have been shown to suppress activated CD4$^+$ T cells (44). The data arising from our experiments of adoptive transfer of CD8$^+$CD122$^+$ T cells into pregnant *Hmox1*$^{+/-}$ female mice confirm the strong regulatory function of these cells during pregnancy, which includes the promotion of placental vascularization and fetal development at midgestation in the absence of placental *Hmox1* expression. Critically, no significant effect of CD8$^+$CD122$^+$ T cell transfer was detectable in WT or *Hmox1*$^{+/-}$ implantations (data not shown), which was expected, as the fetal weight reduction in *Hmox1*$^{+/-}$ implantations was not very profound, thereby limiting the magnitude of reversing effects.

CD8$^+$ cell depletion experiments in stressed mice abrogated the effect of progesterone supplementation on placental function and fetal development. Since CD8$^+$ T cell cytotoxicity in these mice is low, these findings underscore the protective function of CD8$^+$CD122$^+$ T cells during gestation, as depletion of CD8$^+$ cells and, hence, absence of CD8$^+$CD122$^+$ T cells accounted for the failure to successfully support fetal growth.

Strikingly, the generation of CD8$^+$ Tregs has been shown in HMOX-1$^+$ tumors (80). Here, HMOX-1–specific CD8$^+$ Tregs exerted immune-suppressive rather than antitumor functions, suggesting that HMOX-1 may contribute to the development of a tolerogenic environment and may enable the tumor cells to evade rejection by the host's immune system (80). It has been suggested that these HMOX-1–specific CD8$^+$ Tregs exert a more profound suppressive activity compared with CD4$^+$ Tregs. In the context of transplants, HMOX-1–induced modulation of CD8$^+$ T cells has

also been reported, which reduces rejection of organ transplants (81, 82). In the present study, we showed that the generation of $CD8^+CD122^+$ T cells with regulatory function was dependent on *Hmox1* expression in mice. So far, we were not able to determine whether these $CD8^+CD122^+$ T cells are specific for HMOX-1 antigens due to the unavailability of dextramers that are required for detection in mice. Elimination of this technical limitation in the near future will enable elucidation of T cell specificity.

In the current investigation, CoPP-induced HMOX-1 upregulation in vivo resulted in a marked increase of $CD8^+CD122^+$ T cells in nonpregnant female mice. These results provide evidence for the role of HMOX-1 in $CD8^+CD122^+$ T cell generation. Pharmacological HMOX-1 replacement in our model of stress challenge during midgestation could have provided confirmation that HMOX-1 was the primary pathway affected by stress-induced progesterone deficiency. However, HMOX-1 replacement therapies, such as adenoviral gene transfer or the application of CoPP, exert effects that may adversely affect pregnancy maintenance by altering the hypothalamic-pituitary release of hormones (49, 50), suppressing appetite (83), and altering insulin sensitivity in tissues (50). Moreover, the possible teratogenic effects of CoPP have yet to be determined.

Our observation that adoptive transfer of $CD8^+CD122^+$ T cells overcame fetal-growth restriction in *Hmox1*$^{-/-}$ implantations suggests a degree of redundancy with regard to the requirement of placental *Hmox1* expression for fetal development. Furthermore, while HMOX-1 promotes $CD8^+CD122^+$ T cell generation, it does not appear to be necessary for their function during pregnancy, as adoptively transferred $CD8^+CD122^+$ T cells increased vascularization in *Hmox1*$^{-/-}$ placentas.

The results of the present study have potential clinical implications. The detection of low levels of progesterone or an imbalance between cytotoxic and $CD8^+$ Treg subsets prior to the onset of IUGR in human pregnancies could allow the early identification of pregnancies at risk for IUGR. Once these pregnancies are identified, therapeutic interventions aiming to prevent or ameliorate IUGR can be envisioned, such as progesterone supplementation to induce placental HMOX-1 upregulation. To date, progesterone supplementation has been shown to be effective in preventing miscarriage (84) and preterm labor due to a short cervix (85); however, no information is available from placebo-controlled studies on progesterone supplementation in IUGR. The therapeutic approach to directly upregulating placental HMOX-1 expression in pregnancies complicated by IUGR by, e.g., CoPP or adenoviral gene transfer is theoretically also conceivable, although further research is needed to provide insight into possible teratogenic effects. Instead, an upregulation of $CD8^+$ Tregs, which are functionally similar to the $CD8^+CD122^+$ T cell subset we identified in mice, could be envisioned in pregnancies affected by IUGR in the future through extracorporal expansion and adoptive transfer of $CD8^+$ Tregs.

Methods

Animals

Eight-week-old BALB/c female and DBA/2J male mice were purchased from Charles River. BALB/c mice heterozygous for the genetic deletion of HMOX-1 were provided by T.Y. Tsui (University Medical Center Hamburg-Eppendorf). Mice heterozygous for the genetic deletion of *Pgr* were generated on a C57BL6/129SvEv background by J. Lydon (Baylor College of Medicine), as previously described (72). The mice were maintained in an animal facility with a 12-hour light/12-hour dark cycle and food and water provided ad libitum.

Experimental design

To investigate the effect of stress during midgestation, DBA/2J-mated BALB/c females were exposed to 24 hours of sound generated by a rodent repellent device (Conrad Electronics) that consisted of a 70-dB tone lasting 1-second long that was repeated 4 times per minute on gd12.5 and gd14.5. Groups of mice were euthanized on gd12.5, gd13.5, gd14.5, gd15.5, and gd16.5. The *n* of all groups used in the present study is provided in the respective figures. Some of the control and stress-challenged dams were allowed to give birth in order to document gestational length and neonatal weight. To study the role of progesterone and $CD8^+$ cells on stress-induced fetal-growth restriction, some stress-challenged pregnant mice were s.c. injected with the progesterone derivative dihydrodydrogesterone (DHD) (Solvay Pharmaceuticals). Each dam received 1.25 mg of DHD in 0.2 ml of vehicle (20% benzyl benzoate, 80% castor oil) on gd11.5, gd13.5, and gd15.5. Some of the progesterone-supplemented stress-challenged dams were depleted of $CD8^+$ cells (Supplemental Figure 3E) by the i.p. administration of 0.1 mg anti–Lyt 2.1 antibody (BD, catalog 553026) in 0.2 ml PBS on gd10.5, gd11.5, and gd13.5. Control and stressed dams were sham injected employing the corresponding isotype control. On gd16.5, all pregnant BALB/c females were sacrificed.

To study the interaction between progesterone and *Hmox1* during pregnancy, *Pgr*$^{+/-}$ females were mated to *Pgr*$^{+/-}$ male mice. Tissue collection was carried out on gd13.5. Further, *Hmox1*$^{+/-}$ females were mated to *Hmox1*$^{+/-}$ male mice. On gd12.5 a group of dams were adaptively transferred i.v. with 0.3×10^6 $CD8^+CD122^+$ T cells, isolated from lymph nodes and spleen of BALB/c WT mice, in 0.2 ml PBS. Control dams received PBS.

To study the effect of HMOX-1 in vivo induction, virgin 8-week-old BALB/c female mice were administrated 4 times (days 0, 4, 7, and 11) with CoPP (Frontier Scientific Europe) i.p. at 5 mg/kg. CoPP was dissolved in NaOH (0.2 M), adjusted to pH 7.6 with HCl (0.1 M), and diluted in water to obtain a 1 mg/ml stock solution. Control females received PBS. On day 14 after the beginning of CoPP treatment, all animals were euthanized.

At the end point of each experiment, females were anesthetized by CO_2 inhalation, blood samples were collected by retroorbital puncture, and mice were subsequently euthanized. The uterus-draining lymph nodes, placentas, and ovaries were collected, and the fetuses were weighed and fixed in Bouin solution. Following *Hmox1*$^{+/-}$ and *Pgr*$^{+/-}$ mating, fetal tissue samples were collected for genotyping. Depending on the objectives of the experiment, placental tissue was either (a) incubated in RNAlater (Invitrogen) and frozen for subsequent real-time PCR (RT-PCR) analysis, (b) embedded in TissueTek (Sakura) media and frozen for subsequent immunohistochemistry, or (c) weighed and fixed in formalin for subsequent paraffin embedding or MRI analysis.

Cell preparations

Uterus-draining lymph nodes and spleens were processed to obtain single-cell suspensions. Briefly, the tissue was mashed through a 40-μm

cell strainer and washed with PBS. Spleen cell suspensions were further depleted of erythrocytes by incubating with rbc lysis buffer (eBioscience). Cells were washed with PBS and resuspended in FACS buffer (0.5% BSA in PBS). Cell viability and concentration were assessed by counting the Trypan blue negative cells in a hemocytometer.

Immune cell phenotype and cytotoxicity were analyzed in lymph node cells by flow cytometry, as described below. For the cell-transfer experiments, lymph node and spleen cells from gd12.5 dams were pooled to isolate $CD8^+CD122^+$ T cells.

Flow cytometry

Flow-cytometric analyses were carried out following our standard protocol (86). Briefly, 5×10^5 isolated lymphocytes were incubated for 15 minutes in Fc Block solution (0.5% anti-CD16/CD32 antibody, 1% rat normal serum in FACS buffer) to prevent nonspecific binding. After washing, antibodies against specific surface antigens were added at optimal dilutions (Supplemental Table 1), incubated for 30 minutes on ice in the dark, and subsequently washed. For detection of intracellular antigens, cells were fixed and permeabilized using CytoFix/CytoPerm and PermWash buffers (BD Biosciences) according to the manufacturer's instructions. Cells were then incubated for 30 minutes on ice in the dark with the intracellular antibody at dilutions given in Supplemental Table 1. After washing, cells were resuspended in stabilizing fixative (BD Biosciences). Acquisition was performed using FACS Canto II or LSRFortessa (BD Biosciences) cytometers. Instrument settings were compensated using single-color stained samples, and gating thresholds were established based on the "fluorescence minus one" assessments. Data were analyzed using FlowJo software (TreeStar) to investigate positivity for the markers of interest.

Cytotoxicity assays

Intracellular IFN-γ and CD107α cell surface expression were used as markers for $CD8^+$ cell cytotoxicity, according to published protocols (87). In brief, 10^5 lymph node cells in complete RPMI were stimulated by PMA (10 ng/ml) and ionomycin (1 μg/ml). 2% FITC-labeled CD107α antibody (BD, catalog 553793) was added directly to the cells and incubated for 1 hour at 37°C in 5% CO_2. Subsequently, 10 μg/ml Brefeldin A and 6 μg/ml monensin (Golgi-Plug and Golgi-Stop, BD Biosciences) were added into the wells and incubated for an additional 5 hours at 37°C in 5% CO_2. Finally, cells were stained for surface-cell markers and intracellular IFN-γ (BD, catalog 554412) following our standard protocol and analyzed by flow cytometry.

$CD8^+CD122^+$ cell isolation and transfer

Pregnant WT BALB/c female mice between gd11.5 to gd13.5 were used as donors. Single-cell suspensions were prepared from uterus-draining lymph nodes and spleens. $CD8^+$ cells in cell suspensions were enriched by magnetic cell sorting, using the $CD8a^+$ T Cell Isolation Kit for the untouched isolation of mouse $CD8a^+$ T cells (Miltenyi Biotech, catalog 130-104-075). Upon enrichment, cells were stained and $CD8^+CD122^+CD3^+7AAD^-$ cells were isolated employing a FACSAria cell sorter (BD Bioscience). Purity of the cell suspensions was confirmed by subsequent flow cytometry (Supplemental Figure 3F).

Progesterone analysis in serum

Serum progesterone concentrations were determined in accordance with the protocol recommended in a commercially available RIA Kit (MP Biomedicals). The sensitivity of the assay was 0.11 ng/ml for progesterone.

Theiler scoring of fetuses on gd16.5

Fetal development was evaluated by observation of Bouin-fixed fetuses under a Zeiss Stemi 2000-C stereomicroscope. According to Theiler's description (88), the main external features used to differentiate the developmental stages at gd16.5 were fusion of eyelids, degree of divergence in the toes of the hind feet, complexion of the skin, and formation of wrinkles.

PCR determination of *Hmox1* and *Pgr* genotypes

Genomic DNA was isolated from fetal or adult tissue using the DNeasy Kit (QIAGEN) according to the manufacturer's instructions. *Hmox1* and *Pgr* genotypes were determined by PCR employing 2 sets of primers (Supplemental Table 2) in each case. The *Hmox1* WT and mutant alleles were identified as 465 bp and 400 bp PCR products respectively. The *Pgr* WT and mutant alleles generated 856 bp and 580 bp PCR products respectively.

RT-PCR for *Hmox1* mRNA expression and methylation analysis

RNA isolation and cDNA synthesis. Murine placental and ovarian tissue preserved in RNAlater (–20°C) were homogenized using micro packaging vials with ceramic beads (1.4 mm) in the Precellys 24 tissue homogenizer (PeQlab). RNA isolation and subsequent DNA digestion were performed employing the RNeasy Plus Universal Mini Kit (QIAGEN) and the DNA-free Kit (Applied Biosystems). RNA concentration and purity (NanoQuant, Tecan) as well as RNA integrity (Agilent 2100 Bioanalyzer) were assessed. cDNA was synthesized using random primers (Invitrogen). The obtained cDNA was stored at –20°C until further use. Concentration and purity of cDNA were quantified using NanoQuant (Tecan).

Quantification of Hmox1 expression. RT-PCRs were conducted using cDNA as a template. The Applied Biosystems Step One Plus Real-Time PCR Systems and corresponding software were employed in all analysis. A commercially available assay (Applied Biosystems) was used for PCR amplification and detection of *Hmox1* (Mm 00516005_m1), whereas we designed the primers and probe to detect hypoxanthine guanine phosphoribosyl transferase (*Hprt*) (Supplemental Table 3), used as a housekeeping gene. Every sample and target were run in triplicate or quadruplicate. Quantification of the expression of the target gene in relation to the respective housekeeping gene was carried out employing the comparative (ΔΔ) Ct method.

DNA methylation analysis by pyrosequencing. DNA was isolated from RNAlater-preserved tissue using the Nucleospin DNA Kit (Macharey-Nagel). All samples were characterized on a NanoDrop 2000c (ThermoScientific) for purity and concentration of the genomic DNA. Integrity and purity were confirmed on a 0.8% agarose gel. Subsequently, the genomic DNA was treated with bisulfite using the EZ DNA Methylation Kit (Zymo Research) according to the manufacturer's instructions.

The *Hmox1* gene is located on chromosome 8 in mice. Zhao et al. (57) identified 25 CpG dinucleotides around the transcription start site (Supplemental Table 4). Methylation of these CpG positions was analyzed by pyrosequencing on a Pyromark Q24 system (QIAGEN) as described by Freitag et al. (89). The primers were designed using Pyromark Assay Design 2.0 (QIAGEN), using the opposite strand

approach. The area of interest was amplified with the 2 different PCR primer sets (Supplemental Table 5) and subsequently sequenced using primers for shorter ranges of the PCR product (Supplemental Table 6). No data were obtained for CpG23.

Histomorphological and immunohistochemical analyses of placental tissue

Paraffin-embedded placental tissue was cut into 3- to 6-μm histological sections at the midsagittal plane using a microtome (Leica). Similarly frozen embedded placental tissue was cut into 8- to 10-μm histological sections using a cryotome (Microm). Cryosections were placed on aminosilane-coated glass slides (VWR International), fixed in acetone (10 minutes at –20°C), and stored at –20°C after drying.

Masson-Goldner trichrome staining of placental paraffin sections was as follows: tissue sections were deparaffinized, rinsed in distilled water, and dehydrated twice in ethanol (70%). Masson-Goldner Trichrome Staining Kit (VWR International) was used to visualize the morphologically different areas of placental tissue. Briefly, tissue sections were stepwise stained with Weigert's iron hematoxylin, azophloxine staining solution, phosphotungstic acid orange G, and light-green SF solution following the manufacturer's instructions. Finally, the tissue was dehydrated and mounted using Eukitt medium (O. Kindler). Image acquisition was performed using a slide scanner (Mirax Midi, Zeiss). Areas of junctional zone and labyrinth zones were quantified using the program MiraxViewer to calculate a ratio by dividing both values. Furthermore, the level of vascularization was scored (0, low; 3, high) in the labyrinth upon observation of *Hmox1*$^{-/-}$ placenta tissue sections obtained from *Hmox1*$^{+/-}$ matings either upon adoptive transfer with CD8$^+$CD122$^+$ T cells or PBS injections.

Immunohistochemical detection of HMOX-1 and CD34 in placenta section was performed following established protocols (Supplemental Table 7; refs. 86, 90). Briefly, for CD34 staining, paraffin-embedded tissue sections were deparaffinized, rehydrated, and boiled 2 × 10 minutes in citrate buffer pH 6 for epitope retrieval (Supplemental Table 7). Cryosections were used for HMOX-1 staining. Blocking steps were performed following the special needs for each protocol (Supplemental Table 7). For detecting HMOX-1, endogenous peroxidases were quenched by incubation of the tissue sections in 3% H_2O_2 in methanol (Fischer) for 30 minutes. Nonspecific binding of avidin and biotin was blocked by the incubation of the sections with avidin and biotin-blocking solutions (Vector). Each blocking step was followed by washes with TBS. Antibody unspecific binding was prevented by a 30-minute incubation with Protein Blocking Agent (Immunotech) or 10% rabbit serum in AB diluent (Dako), and tissue sections were incubated overnight at 4°C with the primary antibody solution (Supplemental Table 7). After washing, sections were incubated with the solutions containing the secondary antibody specific against the respective first antibody for 1 hour at room temperature and subsequently washed. Tissue sections stained for HMOX-1 were incubated with avidin-biotinylated peroxidase (Vector) (1%) in TBS for 30 minutes, washed, and finally incubated with the substrate solution (H_2O_2/diaminobenzidine in TBS, Dako), which stains the positive cells a brown color. This was followed by a light counterstaining with 0.1% Meyer's hematoxylin (Roth) and rinsing with tap water. Slides were then dehydrated in ethanol (80%, 90%, 96%, 100%) and HistoClear (National Diagnostics) and mounted. CD34 staining was detected with streptavidin-Cy3 in AB diluent, and DAPI was added in the last incubation step (Supplemental Table 7) to counterstain nuclei. After mounting (ImmuMount Media), tissue sections were stored at 4°C for further analysis.

For light immunohistochemistry, image acquisition was performed using a slide scanner (Mirax Midi, Zeiss). Immunofluorescence sections were examined with the fluorescence microscope Zeiss Axioplan and pictures taken with the coupled RT slider spot camera.

CD34$^+$ fetal vessels per visual field were evaluated in areas of high blood perfusion in the labyrinth (Supplemental Figure 1). This analysis required image processing and signal measurements that were performed with Adobe Photoshop CS3 (Adobe Systems). The same settings were applied to all the slides, with the exception of CD34 analysis in gd16.5, for which the contrast was digitally enhanced after recording.

Statistics

For statistical analyses of continuous variables, the independent 2-sample Mann-Whitney *U* test was used when comparing 2 groups. For analyses of 3 or more groups, the Kruskal-Wallis test was employed. The χ^2 test was used to determine whether the distribution of fetuses across TS differs among control and stress-challenged groups. Level of significance was set at $P \leq 0.05$. All statistical analyses were performed with SPSS 19.0 (SPSS Inc.).

Study approval

All animal care and experimental procedures were according to institutional guidelines and conformed to requirements of the German Animal Welfare Act and the Canadian Council of Animal Care. Ethical approvals were obtained from the State Authority of Hamburg (Germany), the Senate for Health, Environment and Consumer Protection Berlin (Germany), and the McMaster University Animal Research Ethics Board (ORG_526; G0251/04; G067/10; AUP# 07B07B48).

Acknowledgments

The authors would like to thank Evelin Hagen, Thomas Andreas, Agnes Wieczorek, Rikst Nynke Verkaik-Schakel, and Josee Plantinga for excellent technical assistance and Kristin Thiele for her valuable contribution in generating this work. This work was supported by research grants from the German Research Foundation (AR232/19–1; to P.C. Arck), the Werner-Otto Foundation (to M.E. Solano), and the Foundation for Research and Science Hamburg (to P.C. Arck and K. Hecher).

Address correspondence to: María Emilia Solano or Petra Clara Arck, University Medical Center Hamburg-Eppendorf, Laboratory for Experimental Feto-Maternal Medicine, Department of Obstetrics and Fetal Medicine, Martinistr. 52, 20246 Hamburg, Germany. Phone: 49.40.7410.52533; E-mail: e.solano@uke.de (M.E. Solano), p.arck@uke.de (P.C. Arck).

1. Romo A, Carceller R, Tobajas J. Intrauterine growth retardation (IUGR): epidemiology and etiology. *Pediatr Endocrinol Rev*. 2009;6(suppl 3):332–336.
2. Mortensen LH, Diderichsen F, Davey Smith G, Nybo Andersen AM. Time is on whose side? Time trends in the association between maternal social disadvantage and offspring fetal growth. A study of 1 409 339 births in Denmark, 1981–2004. *J Epidemiol Community Health*. 2009;63(4):281–285.
3. Beard JR, et al. Socioeconomic and maternal determinants of small-for-gestational age births: patterns of increasing disparity. *Acta Obstet Gyne-*

col Scand. 2009;88(5):575–583.
4. Gould JB, Madan A, Qin C, Chavez G. Perinatal outcomes in two dissimilar immigrant populations in the United States: a dual epidemiologic paradox. *Pediatrics*. 2003;111(6 pt 1):676–682.
5. Chen HY, Chauhan SP, Ward TCS, Mori N, Gass ET, Cisler RA. Aberrant fetal growth and early, late, and postneonatal mortality: an analysis of Milwaukee births, 1996–2007. *Am J Obstet Gynecol*. 2011;204(3):261.e1–261.e10.
6. Barker DJ. The developmental origins of adult disease. *Eur J Epidemiol*. 2003;18(8):733–736.
7. Barker DJ, Osmond C, Simmonds SJ, Wield GA. The relation of small head circumference and thinness at birth to death from cardiovascular disease in adult life. *BMJ*. 1993; 306(6875):422–426.
8. Nepomnyaschy L, Reichman NE. Low birthweight and asthma among young urban children. *Am J Public Health*. 2006;96(9):1604–1610.
9. Thompson JM, Wall C, Becroft DM, Robinson E, Wild CJ, Mitchell EA. Maternal dietary patterns in pregnancy and the association with small-for-gestational-age infants. *Br J Nutr*. 2010;103(11):1665–1673.
10. Campbell MK, Cartier S, Xie B, Kouniakis G, Huang W, Han V. Determinants of small for gestational age birth at term. *Paediatr Perinat Epidemiol*. 2012;26(6):525–533.
11. Lederman SA, et al. The effects of the World Trade Center event on birth outcomes among term deliveries at three lower Manhattan hospitals. *Environ Health Perspect*. 2004;112(17):1772–1778.
12. Arffin F, Al-Bayaty FH, Hassan J. Environmental tobacco smoke and stress as risk factors for miscarriage and preterm births. *Arch Gynecol Obstet*. 2012;286(5):1187–1191.
13. Wadhwa PD, Sandman CA, Porto M, Dunkel-Schetter C, Garite TJ. The association between prenatal stress and infant birth weight and gestational age at birth: a prospective investigation. *Am J Obstet Gynecol*. 1993;169(4):858–865.
14. Lee BE, et al. Psychosocial work stress during pregnancy and birthweight. *Paediatr Perinat Epidemiol*. 2011;25(3):246–254.
15. Dunkel Schetter C. Psychological science on pregnancy: stress processes, biopsychosocial models, and emerging research issues. *Annu Rev Psychol*. 2011;62:531–558.
16. Hobel CJ, Goldstein A, Barrett ES. Psychosocial stress and pregnancy outcome. *Clin Obstet Gynecol*. 2008;51(2):333–348.
17. Baschat AA, HecherK. Fetal growth restriction due to placental disease. *Semin Perinatol*. 2004;28(1):67–80.
18. Murthi P, Kalionis B, Rajaraman G, Keogh RJ, Da Silva Costa F. The role of homeobox genes in the development of placental insufficiency. *Fetal Diagn Ther*. 2012;32(4):225–230.
19. Georgiades P, Ferguson-Smith AC, Burton GJ. Comparative developmental anatomy of the murine and human definitive placentae. *Placenta*. 2002;23(1):3–19.
20. Simmons DG, Rawn S, Davies A, Hughes M, Cross JC. Spatial and temporal expression of the 23 murine Prolactin/Placental Lactogen-related genes is not associated with their position in the locus. *BMC Genomics*. 2008;9:352.
21. Karimi K, Blois SM, Arck PC. The upside of natural killers. *Nat Med*. 2008;14(11):1184–1185.
22. Watson ED, Cross JC. Development of structures and transport functions in the mouse placenta. *Physiology (Bethesda)*. 2005;20:180–193.
23. Mulac-Jericevic B, Mullinax RA, DeMayo FJ, Lydon JP, Conneely OM. Subgroup of reproductive functions of progesterone mediated by progesterone receptor-B isoform. *Science*. 2000;289(5485):1751–1754.
24. Norwitz ER, Lye SJ. Biology of parturition. In: Creasy RK, Resnick R, Iams JD, Lockwood CJ, Moore T, eds. *Creasy and Resnik's Maternal-Fetal Medicine: Principles and Practice*. 6th ed. Philadelphia, Pennsylvania, USA: Elsevier, Inc. 2009:69–85.
25. Blois SM, et al. A pivotal role for galectin-1 in fetomaternal tolerance. *Nat Med*. 2007; 13(12):1450–1457.
26. Arck PC, et al. Early risk factors for miscarriage: a prospective cohort study in pregnant women. *Reprod Biomed Online*. 2008;17(1):101–113.
27. Mucci LA, Lagiou P, Tamimi RM, Hsieh CC, Adami HO, Trichopoulos D. Pregnancy estriol, estradiol, progesterone and prolactin in relation to birth weight and other birth size variables (United States). *Cancer Causes Control.* 2003;14(4):311–318.
28. Hartwig IR, Pincus MK, Diemert A, Hecher K, Arck PC. Sex-specific effect of first-trimester maternal progesterone on birthweight. *Hum Reprod*. 2013;28(1):77–86.
29. Lash GE, et al. Relationship between tissue damage and heme oxygenase expression in chorionic villi of term human placenta. *Am J Physiol Heart Circ Physiol*. 2003;284(1):H160–H167.
30. Zenclussen AC, Joachim R, Hagen E, Peiser C, Klapp BF, Arck PC. Heme oxygenase is down-regulated in stress-triggered and interleukin-12-mediated murine abortion. *Scand J Immunol*. 2002;55(6):560–569.
31. Zhao H, Wong RJ, Kalish FS, Nayak NR, Stevenson DK. Effect of heme oxygenase-1 deficiency on placental development. *Placenta*. 2009;30(10):861–868.
32. Watanabe S, Akagi R, Mori M, Tsuchiya T, Sassa S. Marked developmental changes in heme oxygenase-1 (HO-1) expression in the mouse placenta: correlation between HO-1 expression and placental development. *Placenta*. 2004;25(5):387–395.
33. Chora AA, et al. Heme oxygenase-1 and carbon monoxide suppress autoimmune neuroinflammation. *J Clin Invest*. 2007;117(2):438–447.
34. Mao G, et al. Progesterone increases systemic and local uterine proportions of $CD4^+CD25^+$ Treg cells during midterm pregnancy in mice. *Endocrinology*. 2010; 151(11):5477–5488.
35. Lee JH, Lydon JP, Kim CH. Progesterone suppresses the mTOR pathway and promotes generation of induced regulatory T cells with increased stability. *Eur J Immunol*. 2012;42(10):2683–2696.
36. Hughes GC, Clark EA, Wong AH. The intracellular progesterone receptor regulates $CD4^+$ T cells and T cell-dependent antibody responses. *J Leukoc Biol*. 2013;93(3):369–375.
37. Karimi K, Kandiah N, Chau J, Bienenstock J, Forsythe P. A Lactobacillus rhamnosus strain induces a heme oxygenase dependent increase in $Foxp3^+$ regulatory T cells. *PLoS One*. 2012;7(10):e47556.
38. Aluvihare VR, Kallikourdis M, Betz AG. Regulatory T cells mediate maternal tolerance to the fetus. *Nat Immunol*. 2004;5(3):266–271.
39. Sasaki Y, Sakai M, Miyazaki S, Higuma S, Shiozaki A, Saito S. Decidual and peripheral blood $CD4^+CD25^+$ regulatory T cells in early pregnancy subjects and spontaneous abortion cases. *Mol Hum Reprod*. 2004;10(5):347–353.
40. Erlebacher A, Vencato D, Price KA, Zhang D, Glimcher LH. Constraints in antigen presentation severely restrict T cell recognition of the allogeneic fetus. *J Clin Invest*. 2007;117(5):1399–1411.
41. Shao L, Jacobs AR, Johnson VV, Mayer L. Activation of $CD8^+$ regulatory T cells by human placental trophoblasts. *J Immunol*. 2005;174(12):7539–7547.
42. Tilburgs T, Claas FH, Scherjon SA. Elsevier Trophoblast Research Award Lecture: Unique properties of decidual T cells and their role in immune regulation during human pregnancy. *Placenta*. 2010;31(suppl):S82–S86.
43. Dai Z, et al. Natural $CD8^+CD122^+$ T cells are more potent in suppression of allograft rejection than $CD4^+CD25^+$ regulatory T cells. *Am J Transplant*. 2014;14(1):39–48.
44. Endharti AT, et al. $CD8^+CD122^+$ regulatory T cells (Tregs) and $CD4^+$ Tregs cooperatively prevent and cure $CD4^+$ cell-induced colitis. *J Immunol*. 2011;186(1):41–52.
45. Rifa'i M, Kawamoto Y, Nakashima I, Suzuki H. Essential roles of $CD8^+CD122^+$ regulatory T cells in the maintenance of T cell homeostasis. *J Exp Med*. 2004;200(9):1123–1134.
46. Joachim R, et al. The progesterone derivative dydrogesterone abrogates murine stress-triggered abortion by inducing a Th2 biased local immune response. *Steroids*. 2003;68(10–13):931–940.
47. Sferruzzi-Perri AN, Macpherson AM, Roberts CT, Robertson SA. Csf2 null mutation alters placental gene expression and trophoblast glycogen cell and giant cell abundance in mice. *Biol Reprod*. 2009;81(1):207–221.
48. Barikbin R, et al. Induction of heme oxygenase 1 prevents progression of liver fibrosis in Mdr2 knockout mice. *Hepatology*. 2012;55(2):553–562.
49. Galbraith RA, Krey LC. Cobalt-protoporphyrin suppresses testosterone secretion by multiple interactions within the brain-pituitary-testicular axis. *Neuroendocrinology*. 1989;49(6):641–648.
50. Burgess A, et al. Adipocyte heme oxygenase-1 induction attenuates metabolic syndrome in both male and female obese mice. *Hypertension*. 2010;56(6):1124–1130.
51. Kusinski LC, et al. NOS knockout mouse as a model of fetal growth restriction with an impaired uterine artery function and placental transport phenotype. *Am J Physiol Regul Integr Comp Physiol*. 2012;303(1):R86–R93.
52. Chiossi G, et al. Effect of age and gender on the progression of adult vascular dysfunction in a mouse model of fetal programming lacking endothelial nitric oxide synthase. *Am J Physiol Heart Circ Physiol*. 2011;301(2):H297–H305.
53. Creel S, Winnie JA Jr, Christianson D. Glucocorticoid stress hormones and the effect of predation risk on elk reproduction. *Proc Natl Acad Sci U S A*. 2009;106(30):12388–12393.
54. Erlebacher A, Zhang D, Parlow AF, Glimcher LH.

Ovarian insufficiency and early pregnancy loss induced by activation of the innate immune system. *J Clin Invest*. 2004;114(1):39–48.
55. Abdo M, Hisheh S, Dharmarajan A. Role of tumor necrosis factor-α and the modulating effect of the caspases in rat corpus luteum apoptosis. *Biol Reprod*. 2003;68(4):1241–1248.
56. Care AS, Diener KR, Jasper MJ, Brown HM, Ingman WV, Robertson SA. Macrophages regulate corpus luteum development during embryo implantation in mice. *J Clin Invest*. 2013;123(8):3472–3487.
57. Zhao H, et al. Expression and regulation of heme oxygenase isozymes in the developing mouse cortex. *Pediatr Res*. 2006;60(5):518–523.
58. Lieberman BA, Bona BJ, Edwards DP, Nordeen SK. The constitution of a progesterone response element. *Mol Endocrinol*. 1993;7(4):515–527.
59. Hagerty T, Morgan WW, Elango N, Strong R. Identification of a glucocorticoid-responsive element in the promoter region of the mouse tyrosine hydroxylase gene. *J Neurochem*. 2001;76(3):825–834.
60. Vandevyver S1, Dejager L, Tuckermann J, Libert C. New insights into the anti-inflammatory mechanisms of glucocorticoids: an emerging role for glucocorticoid-receptor-mediated transactivation. *Endocrinology*. 2013;154(3):993–1007.
61. Burek M, Steinberg K, Förster CY. Mechanisms of transcriptional activation of the mouse claudin-5 promoter by estrogen receptor alpha and beta. *Mol Cell Endocrinol*. 2014;392(1–2):144–151.
62. Chi PL, Lin CC, Chen YW, Hsiao LD, Yang CM. CO induces Nrf2-dependent heme oxygenase-1 transcription by cooperating with Sp1 and c-Jun in rat brain astrocytes [published online ahead of print August 23, 2014]. *Mol Neurobiol*. doi:10.1007/s12035-014-8869-4.
63. Zhao H, Azuma J, Kalish F, Wong RJ, Stevenson DK. Maternal heme oxygenase 1 regulates placental vasculature development via angiogenic factors in mice. *Biol Reprod*. 2011;85(5):1005–1012.
64. Acevedo CH, Ahmed A. Hemeoxygenase-1 inhibits human myometrial contractility via carbon monoxide and is upregulated by progesterone during pregnancy. *J Clin Invest*. 1998;101(5):949–955.
65. Eide IP, Isaksen CV, Salvesen KA, Langaas M, Schonberg SA, Austgulen R. Decidual expression and maternal serum levels of heme oxygenase 1 are increased in pre-eclampsia. *Acta Obstet Gynecol Scand*. 2008;87(3):272–279.
66. Ahmed A, et al. Induction of placental heme oxygenase-1 is protective against TNFα-induced cytotoxicity and promotes vessel relaxation. *Mol Med*. 2000;6(5):391–409.
67. Barber A, Robson SC, Myatt L, Bulmer JN, Lyall F. Heme oxygenase expression in human placenta and placental bed: reduced expression of placenta endothelial HO-2 in preeclampsia and fetal growth restriction. *FASEB J*. 2001;15(7):1158–1168.
68. McLaughlin BE, et al. Heme oxygenase expression in selected regions of term human placenta. *Exp Biol Med (Maywood)*. 2003;228(5):564–567.
69. Yachie A, et al. Oxidative stress causes enhanced endothelial cell injury in human heme oxygenase-1 deficiency. *J Clin Invest*. 1999;103(1):129–135.
70. Fernandez-Valdivia R, et al. Revealing progesterone's role in uterine and mammary gland biology: insights from the mouse. *Semin Reprod Med*. 2005;23(1):22–37.
71. Szekeres-Bartho J, Szekeres G, Debre P, Autran B, Chaouat G. Reactivity of lymphocytes to a progesterone receptor-specific monoclonal antibody. *Cell Immunol*. 1990;125(2):273–283.
72. Lydon JP, et al. Mice lacking progesterone receptor exhibit pleiotropic reproductive abnormalities. *Genes Dev*. 1995;9(18):2266–2278.
73. Ohta Y, et al. A single exposure of rats to water-immersion restraint stress induces oxidative stress more severely in the thymus than in the spleen. *Redox Rep*. 2012;17(5):200–205.
74. Perchellet AL, Jasti S, Petroff MG. Maternal $CD4^+$ and $CD8^+$ T cell tolerance towards a fetal minor histocompatibility antigen in T cell receptor transgenic mice. *Biol Reprod*. 2013;89(4):102.
75. Arck PC, Merali FS, Manuel J, Chaouat G, Clark DA. Stress-triggered abortion: inhibition of protective suppression and promotion of tumor necrosis factor-alpha (TNF-α) release as a mechanism triggering resorptions in mice. *Am J Reprod Immunol*. 1995;33(1):74–80.
76. Dai H, Wan N, Zhang S, Moore Y, Wan F, Dai Z. Cutting edge: programmed death-1 defines $CD8^+CD122^+$ T cells as regulatory versus memory T cells. *J Immunol*. 2010;185(2):803–807.
77. Kim HJ, Verbinnen B, Tang X, Lu L, Cantor H. Inhibition of follicular T-helper cells by CD8(+) regulatory T cells is essential for self tolerance. *Nature*. 2010;467(7313):328–332.
78. Rifa'i M, et al. $CD8^+CD122^+$ regulatory T cells recognize activated T cells via conventional MHC class I-αβTCR interaction and become IL-10-producing active regulatory cells. *Int Immunol*. 2008;20(7):937–947.
79. Shi Z, Rifa'i M, Lee YH, Shiku H, Isobe K, Suzuki H. Importance of CD80/CD86-CD28 interactions in the recognition of target cells by $CD8^+CD122^+$ regulatory T cells. *Immunology*. 2008;124(1):121–128.
80. Andersen MH, Sørensen RB, Brimnes MK, Svane IM, Becker JC, thor Straten P. Identification of heme oxygenase-1-specific regulatory $CD8^+$ T cells in cancer patients. *J Clin Invest*. 2009;119(8):2245–2256.
81. Clarke HM, Shrivastava S, Motterlini R, Sawle P, Chen D, Dorling A. Donor HO-1 expression inhibits intimal hyperplasia in unmanipulated graft recipients: a potential role for CD8+ T-cell modulation by carbon monoxide. *Transplantation*. 2009;88(5):653–661.
82. Martins PN, et al. Induction of heme oxygenase-1 in the donor reduces graft immunogenicity. *Transplant Proc*. 2005;37(1):384–386.
83. Galbraith RA, Kappas A. Regulation of food intake and body weight by cobalt porphyrins in animals. *Proc Natl Acad Sci U S A*. 1989;86(19):7653–7657.
84. Wahabi HA, Fayed AA, Esmaeil SA, Al Zeidan RA. Progestogen for treating threatened miscarriage. *Cochrane Database Syst Rev*. 2011;(12):CD005943.
85. Romero R. Vaginal progesterone to reduce the rate of preterm birth and neonatal morbidity: a solution at last. *Womens Health (Lond Engl)*. 2011;7(5):501–504.
86. Solano ME, Sander VA, Ho H, Motta AB, Arck PC. Systemic inflammation, cellular influx and up-regulation of ovarian VCAM-1 expression in a mouse model of polycystic ovary syndrome (PCOS). *J Reprod Immunol*. 2011;92(1–2):33–44.
87. Karimi K, et al. Regulation of pregnancy maintenance and fetal survival in mice by CD27(low) mature NK cells. *J Mol Med (Berl)*. 2012;90(9):1047–1057.
88. Theiler K. *The House Mouse - Atlas of Embryonic Development*. Edinburgh, United Kingdom: Springer-Verlag; 1972.
89. Freitag N, et al. Influence of relative NK-DC abundance on placentation and its relation to epigenetic programming in the offspring. *Cell Death Dis*. 2014;5:e1392.
90. Horst AK, et al. CEACAM1+ myeloid cells control angiogenesis in inflammation. *Blood*. 2009;113(26):6726–6736.